*Journal of Global Positioning Systems (2005)*
*Vol. 4, No. 1-2: 12-26*

Journal of Global Positioning Systems
2005
© CPGPS

# An Integrated Position and Attitude Determination System to Support Real-Time, Mobile, Augmented Reality Applications

**Allison Kealy & Stephen Scott-Young**

Department of Geomatics, The University of Melbourne, Victoria, Australia
Tel: +61 (0)3 8344 6804 Fax: + 61 (0)3 9347 2916, Email: akealy@unimelb.edu.au

Received: 6 December 2004 / Accepted: 26 October 2005

**Abstract.** Augmented reality (AR) technologies enable digitally stored information (virtual objects) to be overlaid graphically on views of the real world. As such, they are able to significantly enhance decision-making and operational efficiency in complex environments. AR technologies typically comprise a fusion of positioning and attitude sensors with visualisation capability and an information processing system. The decreasing size and cost of visualisation and positioning hardware and the increasing portable processing power of laptop and handheld computers now offer enormous potential for the development of intelligent solutions based around real-time, mobile AR technologies.

For any application built around AR technologies, its effectiveness lies in the accuracy to which the virtual objects can be aligned with views of the real world. For many of these applications, this is directly a function of the accuracy to which the position and orientation of the operation platform can be determined. This paper presents an integrated positioning system that combines an array of dual frequency GPS receivers, a fibre optic gyroscope and vehicle odometer within a centralised Kalman filter. It assesses the accuracy of the filter outputs of position and attitude as appropriate to supporting real-time, mobile AR applications. The design and testing of an AR prototype that combines the Kalman filter state with real-time imagery containing augmented objects will also be presented. Finally, approaches adopted to tune the filter and reduce inherent sensor noise, as well as results from a case study undertaken within the land mobile environment will be described.

**Key words:** Augmented Reality, GPS, Inertial Sensors, Kalman Filter, Integrated Systems

## 1 Introduction

Over the last decade there has been an increasing trend towards the development of complex decision making systems that utilise spatial information. Whilst this has largely been attributed to developments in the fundamental technologies used to acquire, analyse and visualise spatial data, parallel developments in enabling technologies such as mobile computing and wired and wireless communications have also contributed significantly to increasing the diversity of applications and users that rely on spatial information.

This research investigates the use of Augmented Reality (AR) technologies as an innovative approach to presenting spatial information in an understandable, user-friendly way through an enhancement of a user's real-world perspective view. AR technology is not new and has already experienced some success in many areas such as powerplant maintenance procedures (Klinker *et al.*, 2001) and cardiac surgery (Devernay *et al.*, 2001), However, current generation AR systems suffer from many limitations. These include display systems that are often difficult to view in a wide range of environments (particularly outdoors); delays in displaying augmented information at the appropriate time or position caused by the time required to process data from the AR sensors and its databases; a time consuming calibration process of the AR sensors; a lack of interactivity between the user and the AR system; and difficulties in determining the location of the user in outdoor environments without the prior preparation of placing markers with known locations around the area (Azuma *et al.*, 2001).

The limitations of AR operation in unprepared environments forms the basis of the research problem addressed in this paper, that is, to develop a position and attitude determination component for AR systems capable of operation in unprepared environments. In particular, it investigates the integration of measurements

from the Global Positioning System (GPS) and Dead Reckoning (DR) with intelligent information obtained from map matching techniques to enable the continuous and accurate real-time visual alignment of three-dimensional objects within the perspective view of a user operating in outdoor unprepared environments.

This paper presents the details of the Kalman filtering algorithm developed to calculate the position and attitude parameters, as well as the approaches adopted to "tune" and "constrain" the Kalman filter solution for operation within the land mobile environment. Practical test results using an AR prototype developed within this research are also presented to validate the performance of the integration algorithms.

## 2 Position and attitude determination

AR systems rely on position and attitude parameters to register augmented objects with the "real world" environment. The accuracy with which these parameters can be determined, as well as the availability of the solution, can have a significant effect on the success of the AR system as a whole.

To determine accurate and continuous outputs of position and attitude parameters (heading, pitch and roll), this research investigates the performance of an integrated system comprising an array of three Leica GPS 530® receivers operating in a Real Time Kinematic (RTK) mode, a fibre optic gyroscope and an odometer, see Figure 1.

Each GPS receiver is configured to transmit the GGA NMEA string 10 times per second to a processor (laptop computer). The fibre optic gyroscope is configured to output the rate of change of direction of the platform. It is also possible to connect the gyroscope to the engine computer management system of the land mobile platform used in this research and thereby obtain outputs of the distance travelled. The on-board processor was used to synchronise the measurements from all sensors, to collate the data and to calculate in real-time the position and attitude parameters.

To obtain optimal estimates of the position and attitude parameters required for the AR system developed in this research, a loosely coupled Kalman filter was used to integrate the measurements obtained from all available sensors with the geometric distances of the fixed antenna geometry and the spatial intelligence of a road network database accessed through map matching techniques.

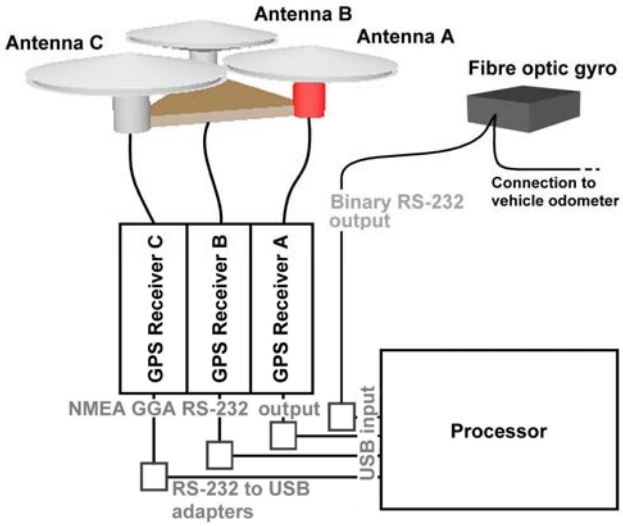


Figure 1 Schematic diagram of the hardware and the flow of data of the integrated positioning and attitude determination system

### 2.1 Reference Frames

To compute the attitude parameters for the mobile platform, the three GPS antennae (A, B, C) are used to define a platform reference frame. Figure 2 illustrates the GPS antennae configuration and the platform reference frame defined. The vector BC defines the pitch axis, the vector AD defines the roll axis, and the vector through D and perpendicular to the plane defined by the points A, B and C defines the heading axis. Antenna A acts as the platform origin and provides the position of the platform. A positive pitch rotation occurs when the platform tilts back (i.e., the front of the platform rises). A positive roll rotation occurs when the platform tilts to the right side, and a positive heading rotation occurs when the platform rotates to the right. For notation purposes, the platform reference frame axes are labelled with a subscript 'A' (originating from the fact that the platform reference frame is defined by the antennae). For computational efficiency the Geocentric Cartesian coordinates obtained from the GPS receivers are converted to the model reference frame (which is a local reference frame) with components referred to East, North and Up (EM, NM, UM) via a rotation matrix.

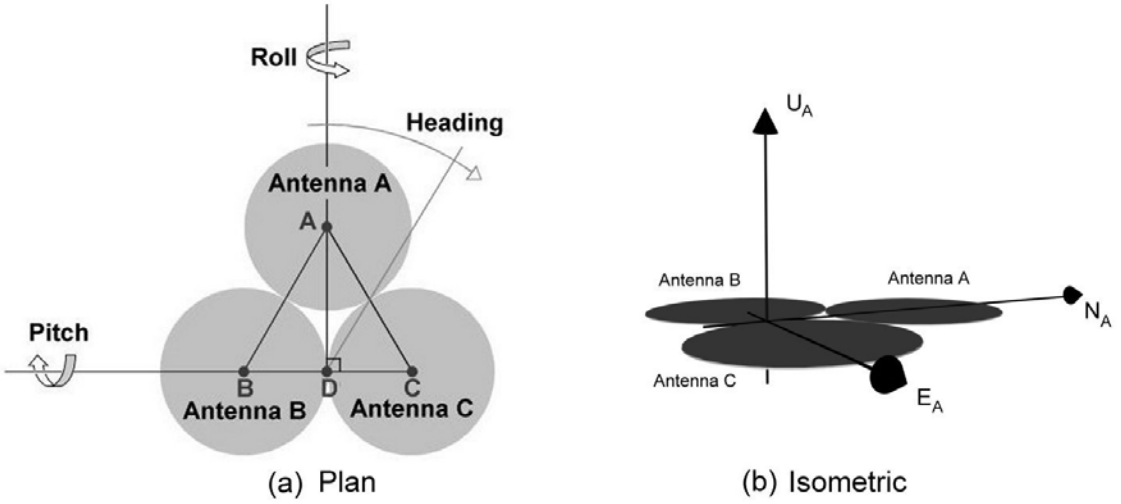


Figure 2 The platform reference frame: (a) roll, pitch and heading as defined by the fixed relative position of the three antennae A, B, and C, and (b) antennae referenced within an East, North and Up platform reference frame

### 2.2 Kalman filter integration models

To compute the position and attitude parameters for the mobile AR system, a Kalman filter was used to integrate the measurements obtained from the array of GPS antennae with those from the gyroscope and the odometer. As specific details on Kalman filtering algorithms and their implementations can be found in many references (eg Cross, 1990 and Logan, 2000), this paper focuses on the specification of the Kalman filter models generated for the AR prototype developed in this research.

#### 2.2.1 Kalman filter functional model for the GPS observations

The approach taken in this research was to define the unknowns (or state, $\bar{x}_i$) to be solved, as the platform position in the model reference frame (i.e. the position of Antenna A ($\begin{bmatrix}\bar{E} & \bar{N} & \bar{U}\end{bmatrix}$, the master antenna) and the attitude parameters (i.e. heading, pitch and roll, $\begin{bmatrix}h & p & r\end{bmatrix}$), as presented in Equation (1).

$$\bar{x}_i = \begin{bmatrix}\bar{E} & \bar{N} & \bar{U} & \bar{h} & \bar{p} & \bar{r}\end{bmatrix}^T \quad (1)$$

The observations are the coordinates of the each of the GPS antennae in the model reference frame. To constrain the solution, the fixed spatial relationships between the GPS antennae are also included and are defined as offsets in Easting, Northing and Up of Antennae B and C from Antenna A, see Figure 3. Note that the platform reference frame has been defined in such a way that the offsets in altitude (i.e. the Up component in the platform reference frame) between the antennae are zero. Due to the high precision (approximately 0.2 millimetres) with which these offsets can be calculated using photogrammetric techniques and, since the antennae are rigidly fixed to the platform, the offsets are treated as constants.

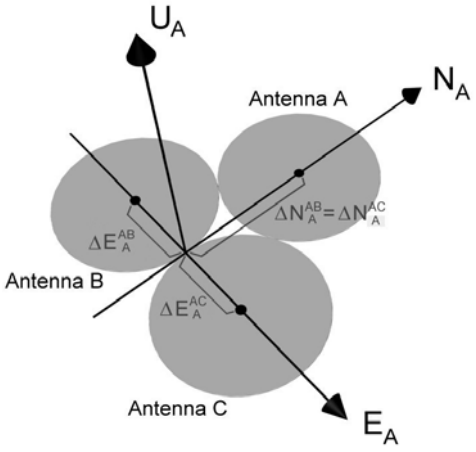


Figure 3 The spatial relationship between the antennae in the platform reference frame

The coordinates of Antennae A, B and C in the model reference frame can be defined in terms of the coordinates of Antenna A, the offsets between the antennae (defined in the platform reference frame), and the attitude (heading, pitch and roll) of the platform within the model reference frame. Hence:

$$A_M = \begin{bmatrix} E_M^A \\ N_M^A \\ U_M^A \end{bmatrix}$$

$$B_M = A_M + R_A^M \begin{bmatrix} \Delta E_A^{AB} \\ \Delta N_A^{AB} \\ \Delta U_A^{AB} \end{bmatrix} = \begin{bmatrix} E_M^A \\ N_M^A \\ U_M^A \end{bmatrix} + R_A^M \begin{bmatrix} \Delta E_A^{AB} \\ \Delta N_A^{AB} \\ \Delta U_A^{AB} \end{bmatrix} \qquad (2)$$

$$C_M = A_M + R_A^M \begin{bmatrix} \Delta E_A^{AC} \\ \Delta N_A^{AC} \\ \Delta U_A^{AC} \end{bmatrix} = \begin{bmatrix} E_M^A \\ N_M^A \\ U_M^A \end{bmatrix} + R_A^M \begin{bmatrix} \Delta E_A^{AC} \\ \Delta N_A^{AC} \\ \Delta U_A^{AC} \end{bmatrix}$$

where $R_A^M$ is a rotation matrix that defines the rotation between the platform reference frame and the model reference frame. The rotation angles are simply the attitude parameters.

From Equations (2), the observation equations for the GPS measurements can be derived in the standard least squares observation equation form $F(\bar{x}) = \bar{l}$ (Equations (5)), where $\bar{x}$ is the vector of unknowns and $\bar{l}$ is the vector of observations. Note that from this point onwards unless otherwise indicated, values in the least squares adjustment equations without a subscript 'M' are in the model reference frame, allowing clearer use of subscripts to identify Kalman filter epoch values and predicted quantities.

### 2.2.1 Kalman filter dynamic model

For implementation of the Kalman filter, the vector of unknowns $\bar{x}$, must also include sufficient parameters to enable prediction of the platform state from one epoch to the next by modelling the mobile platform dynamics. Hence, 13 additional parameters (see Equation (3)) are introduced.

In this research, a polynomial model is used to predict heading, pitch, roll and velocity from one epoch to the next, while position is predicted using standard three-dimensional dead reckoning (DR) equations. The full dynamic model used in this research is shown in Equation (4).

The polynomial dynamic model for both heading and velocity are two orders higher than that of roll and pitch to cater for more frequent and larger magnitude changes in these parameters as would be expected from a land vehicle. Noise in the dynamic model is assigned within the Kalman filter through variances for the parameters $\dddot{h}$, $\ddot{p}$, $\ddot{r}$ and $\dddot{v}$.

### 2.2.3 Kalman filter functional model for the gyroscope and odometer

Similar to the GPS outputs, to develop the gyroscope and odometer observations equations, the measurements from these instruments are modelled in terms of the unknowns. For this project, the gyroscope is used to measure change in heading, while the odometer measures the distance travelled between measurement epochs. Thus, the observation equation model for the Kalman filter now contains two additional observations, and two additional observation equations. The unknown parameters in the Kalman filter are also increased by two to account for the inherent sensor biases of gyro drift rate and the odometer scale factor.

Equations (5) present the full functional models for all observations in the integrated positioning and attitude determination system developed in this research.

Where, $f_1(\bar{x},\bar{l})$ to $f_9(\bar{x},\bar{l})$ are the observation equations from the GPS antenna array. $f_{10}(\bar{x},\bar{l})$ to $f_{28}(\bar{x},\bar{l})$ are derived from the predictions within the Kalman filter and $f_{29}(\bar{x},\bar{l})$ to $f_{32}(\bar{x},\bar{l})$ are the observation equations derived from the gyroscope and odometer measurements, where;

$\dot{\beta}$ Gyro drift rate error (deg/s)

$\varepsilon$ Odometer scale factor error

$\dot{h}$ Change in heading as measured by the gyro (deg)

$d$ Distance travelled as measured by the odometer (m)

### 2.3 Tuning the Kalman filter

When implementing the Kalman filter, information about observation precisions, as well as the magnitude of noise in the dynamic model is required. In defining the dynamic model, estimates of variances for $\dddot{h}$, $\ddot{p}$, $\ddot{r}$ and $\dddot{v}$ are required. If the sizes of these estimates are large compared to the variances given to the observations, a slow reaction to sharp manoeuvres occurs. If the sizes of these estimates are small compared to the variances given to the observations, a quick reaction to sharp manoeuvres occurs. In an operational environment neither of these situations is ideal, and a model that applies increased smoothing when the dynamics of the antennae are relatively static and a quick reaction time when the dynamics of the antennae change rapidly would be more suitable. Within this research, this methodology of "smart stochastic modelling" is achieved through the implementation of a standard least squares unit variance confidence test at each epoch.

$$\bar{x}_i = \left[ \bar{E} \;\; \bar{N} \;\; \bar{U} \;\; \bar{h} \;\; \bar{p} \;\; \bar{r} \;\; \bar{v} \;\; \bar{\dot{h}} \;\; \bar{\dot{p}} \;\; \bar{\dot{r}} \;\; \bar{\dot{v}} \;\; \bar{\ddot{h}} \;\; \bar{\ddot{p}} \;\; \bar{\ddot{r}} \;\; \bar{\ddot{v}} \;\; \bar{\dddot{h}} \;\; \bar{\dddot{p}} \;\; \bar{\dddot{h}} \;\; \bar{\dddot{v}} \right]^T \tag{3}$$

$$
\begin{aligned}
{}_p h_i &= h_{i-1} + \dot{h}_{i-1}\Delta t + \frac{1}{2}\ddot{h}_{i-1}\Delta t^2 + \frac{1}{6}\dddot{h}_{i-1}\Delta t^3 + \frac{1}{24}\bar{\dddot{h}}_{i-1}\Delta t^4 \\
{}_p \dot{h}_i &= +\dot{h}_{i-1} + \ddot{h}_{i-1}\Delta t + \frac{1}{2}\dddot{h}_{i-1}\Delta t^2 + \frac{1}{6}\bar{\dddot{h}}_{i-1}\Delta t^3 \\
{}_p \ddot{h}_i &= \ddot{h}_{i-1} + \dddot{h}_{i-1}\Delta t + \bar{\dddot{h}}_{i-1}\frac{1}{2}\Delta t^2 \\
{}_p \dddot{h}_i &= \dddot{h}_{i-1} + \bar{\dddot{h}}_{i-1}\Delta t \\
{}_p \bar{\dddot{h}}_i &= \bar{\dddot{h}}_{i-1} \\
{}_p p_i &= p_{i-1} + \dot{p}_{i-1}\Delta t + \frac{1}{2}\ddot{p}_{i-1}\Delta t^2 \\
{}_p \dot{p}_i &= \dot{p}_{i-1} + \ddot{p}_{i-1}\Delta t \\
{}_p \ddot{p}_i &= \ddot{p}_{i-1} \\
{}_p r_i &= r_{i-1} + \dot{r}_{i-1}\Delta t + \frac{1}{2}\ddot{r}_{i-1}\Delta t^2 \\
{}_p \dot{r}_i &= \dot{r}_{i-1} + \ddot{r}_{i-1}\Delta t \\
{}_p \ddot{r}_i &= \ddot{r}_{i-1} \\
{}_p v_i &= v_{i-1} + \dot{v}_{i-1}\Delta t + \frac{1}{2}\ddot{v}_{i-1}\Delta t^2 + \frac{1}{6}\dddot{v}_{i-1}\Delta t^3 + \frac{1}{24}\bar{\dddot{v}}_{i-1}\Delta t^4 \\
{}_p \dot{v}_i &= \dot{v}_{i-1} + \ddot{v}_{i-1}\Delta t + \frac{1}{2}\dddot{v}_{i-1}\Delta t^2 + \frac{1}{6}\bar{\dddot{v}}_{i-1}\Delta t^3 \\
{}_p \ddot{v}_i &= \ddot{v}_{i-1} + \dddot{v}_{i-1}\Delta t + \frac{1}{2}\bar{\dddot{v}}_{i-1}\Delta t^2 \\
{}_p \dddot{v}_i &= \dddot{v}_{i-1} + \bar{\dddot{v}}_{i-1}\Delta t \\
{}_p \bar{\dddot{v}}_i &= \bar{\dddot{v}}_{i-1} \\
{}_p E_i &= E_{i-1} + {}_p v_i \Delta t \cos({}_p p_i)\sin({}_p h_i) \\
{}_p N_i &= N_{i-1} + {}_p v_i \Delta t \cos({}_p p_i)\cos({}_p h_i) \\
{}_p U_i &= U_{i-1} + {}_p v_i \Delta t \sin({}_p p_i)
\end{aligned}
\tag{4}
$$

where:

| | |
|---|---|
| E | Easting coordinate (m) |
| N | Northing coordinate (m) |
| U | Up coordinate (m) |
| h | Heading (deg) |
| p | Pitch (deg) |
| r | Roll (deg) |
| v | Velocity (m/s) |
| $\dot{h}$ | Change in h (deg/s) |
| $\dot{p}$ | Change in p (deg/s) |
| $\dot{r}$ | Change in r (deg/s) |
| $\dot{v}$ | Change in v (deg/s$^2$) (otherwise known as acceleration) |
| $\ddot{h}$ | Change in $\dot{h}$ (deg/s$^2$) |
| $\ddot{p}$ | Change in $\dot{p}$ (deg/s$^2$) |
| $\ddot{r}$ | Change in $\dot{r}$ (deg/s$^2$) |
| $\ddot{v}$ | Change in $\dot{v}$ (deg/s$^3$) (otherwise known as jerk) |
| $\dddot{h}$ | Change in $\ddot{h}$ (deg/s$^3$) |
| $\dddot{v}$ | Change in $\ddot{v}$ (deg/s$^4$) |
| $\bar{\dddot{h}}$ | Change in $\dddot{h}$ (deg/s$^4$) |
| $\bar{\dddot{v}}$ | Change in $\dddot{v}$ (deg/s$^5$) |

Note that for these equations, a subscript 'p' denotes a predicted quantity, while a subscript 'i' denotes the current measurement epoch.

### 2.3.1 Unit variance confidence test

The unit variance $\left(\sigma_0^2\right)$ is a function of the least squares residuals ($\hat{v}$) (the difference between the measurements and the updated measurements after the Kalman filter process), the variance of the measurements ($V_1$), and the degrees of freedom of the adjustment (df) (Equation (6)).

$$\sigma_0{}^2 = \frac{\hat{v}^T V_l \hat{v}}{df} \tag{6}$$

Given the correct selection of measurement variances and the absence of gross errors, the unit variance should not differ significantly from unity. In this research, the unit variance confidence test was applied at each epoch to distinguish actual movement of the vehicle platform from apparent movement caused by noise in the observations. In particular, the test seeks to determine when the dynamic model correctly predicts the motion of the vehicle. If the unit variance confidence test fails, this is used as an indication that the variances of the dynamic model predicted observations are overestimated. It can then be assumed that:

- the dynamic model is not successfully predicting the movement of the platform to the precision indicated by the predicted observations variances, and therefore;
- the Kalman filter has failed to respond to a movement of the platform.

Consequently, the weights in the Kalman filter are significantly reduced to allow the filter to catch up to the current platform attitude. On the other hand, if the unit variance confidence test does not differ significantly from unity:

- the dynamic model is successfully predicting the movement of the platform to the precision indicated by the predicted observation variances, and
- the Kalman filter is sufficiently reacting to vehicle dynamics.

Hence, the filter variances remain high (or are increased if they were previously lowered) to provide maximum filtering of the data and removal of noise.

$$\bar{x}_i = \left[ \bar{E} \;\; \bar{N} \;\; \bar{U} \;\; \bar{h} \;\; \bar{p} \;\; \bar{r} \;\; \bar{v} \;\; \dot{\bar{h}} \;\; \dot{\bar{p}} \;\; \dot{\bar{r}} \;\; \dot{\bar{v}} \;\; \ddot{\bar{h}} \;\; \ddot{\bar{p}} \;\; \ddot{\bar{r}} \;\; \ddot{\bar{v}} \;\; \dddot{\bar{h}} \;\; \dddot{\bar{p}} \;\; \dddot{\bar{h}} \;\; \dddot{\bar{v}} \;\; \dot{\bar{\beta}} \;\; \dot{\bar{\varepsilon}} \right]^T$$

$$l_i = \left[ P_i \quad e_i \right]^T$$

$$P_i = \left[ {}_p\bar{E} \;\; {}_p\bar{N} \;\; {}_p\bar{U} \;\; {}_p\bar{h} \;\; {}_p\bar{p} \;\; {}_p\bar{r} \;\; {}_p\bar{v} \;\; {}_p\dot{\bar{h}} \;\; {}_p\dot{\bar{p}} \;\; {}_p\dot{\bar{r}} \;\; {}_p\dot{\bar{v}} \;\; {}_p\ddot{\bar{h}} \;\; {}_p\ddot{\bar{p}} \;\; {}_p\ddot{\bar{r}} \;\; {}_p\ddot{\bar{v}} \;\; {}_p\dddot{\bar{h}} \;\; {}_p\dddot{\bar{p}} \;\; {}_p\dddot{\bar{h}} \;\; {}_p\dddot{\bar{v}} \;\; {}_p\dot{\bar{\beta}} \;\; {}_p\dot{\bar{\varepsilon}} \right]^T$$

$$e_i = \left[ E^A \;\; N^A \;\; U^A \;\; E^B \;\; N^B \;\; U^B \;\; E^C \;\; N^C \;\; U^C \;\; \dot{h} \;\; d \right]^T$$

$$\begin{aligned}
f_1(\bar{x},\bar{l}) &= \bar{E} \\
f_2(\bar{x},\bar{l}) &= \bar{N} \\
f_3(\bar{x},\bar{l}) &= \bar{U} \\
f_4(\bar{x},\bar{l}) &= \bar{E} + \left(\cos(\bar{r})\cos(\bar{h}) + \sin(\bar{r})\sin(\bar{p})\sin(\bar{h})\right)\Delta E_A^{AB} + \\
&\quad \left(\cos(\bar{p})\sin(\bar{h})\right)\Delta N_A^{AB} + \\
&\quad \left(\sin(\bar{r})\cos(\bar{h}) - \cos(\bar{r})\sin(\bar{p})\sin(\bar{h})\right)\Delta U_A^{AB} \\
f_5(\bar{x},\bar{l}) &= \bar{N} + \left(-\cos(\bar{r})\sin(\bar{h}) + \sin(\bar{r})\sin(\bar{p})\cos(\bar{h})\right)\Delta E_A^{AB} + \\
&\quad \left(\cos(\bar{p})\cos(\bar{h})\right)\Delta N_A^{AB} + \\
&\quad \left(-\sin(\bar{r})\sin(\bar{h}) - \cos(\bar{h})\cos(\bar{r})\sin(\bar{p})\right)\Delta U_A^{AB} \\
f_6(\bar{x},\bar{l}) &= \bar{U} + \left(-\sin(\bar{r})\cos(\bar{p})\right)\Delta E_A^{AB} + \\
&\quad \sin(\bar{p})\Delta N_A^{AB} + \\
&\quad \cos(\bar{r})\cos(\bar{p})\Delta U_A^{AB} \\
f_7(\bar{x},\bar{l}) &= \bar{E} + \left(\cos(\bar{r})\cos(\bar{h}) + \sin(\bar{r})\sin(p)\sin(\bar{h})\right)\Delta E_A^{AC} + \\
&\quad \left(\cos(\bar{p})\sin(\bar{h})\right)\Delta N_A^{AC} + \\
&\quad \left(\sin(\bar{r})\cos(\bar{h}) - \cos(\bar{r})\sin(\bar{p})\sin(\bar{h})\right)\Delta U_A^{AC} \\
f_8(\bar{x},\bar{l}) &= \bar{N} + \left(-\cos(\bar{r})\sin(\bar{h}) + \sin(\bar{r})\sin(\bar{p})\cos(\bar{h})\right)\Delta E_A^{AC} + \\
&\quad \left(\cos(\bar{p})\cos(\bar{h})\right)\Delta N_A^{AC} + \\
&\quad \left(-\sin(\bar{r})\sin(\bar{h}) - \cos(\bar{h})\cos(\bar{r})\sin(\bar{p})\right)\Delta U_A^{AC} \\
f_9(\bar{x},\bar{l}) &= \bar{U} + \left(-\sin(\bar{r})\cos(\bar{p})\right)\Delta E_A^{AC} + \\
&\quad \sin(\bar{p})\Delta N_A^{AC} + \\
&\quad \cos(\bar{r})\cos(\bar{p})\Delta U_A^{AC}
\end{aligned} \tag{5}$$

$$f_{10}(\bar{x},\bar{l}) = \bar{E} \quad f_{11}(\bar{x},\bar{l}) = \bar{N} \quad f_{12}(\bar{x},\bar{l}) = \bar{U} \quad f_{13}(\bar{x},\bar{l}) = \bar{h} \quad f_{14}(\bar{x},\bar{l}) = \bar{p} \quad f_{15}(\bar{x},\bar{l}) = \bar{r}$$
$$f_{16}(\bar{x},\bar{l}) = \bar{v} \quad f_{17}(\bar{x},\bar{l}) = \dot{\bar{h}} \quad f_{18}(\bar{x},\bar{l}) = \dot{\bar{p}} \quad f_{19}(\bar{x},\bar{l}) = \dot{\bar{r}} \quad f_{20}(\bar{x},\bar{l}) = \dot{\bar{v}} \quad f_{21}(\bar{x},\bar{l}) = \ddot{\bar{h}}$$
$$f_{22}(\bar{x},\bar{l}) = \ddot{\bar{p}} \quad f_{23}(\bar{x},\bar{l}) = \ddot{\bar{r}} \quad f_{24}(\bar{x},\bar{l}) = \ddot{\bar{v}} \quad f_{25}(\bar{x},\bar{l}) = \dddot{\bar{h}} \quad f_{26}(\bar{x},\bar{l}) = \dddot{\bar{v}} \quad f_{27}(\bar{x},\bar{l}) = \dddot{\bar{h}}$$
$$f_{28}(\bar{x},\bar{l}) = \dddot{\bar{v}}$$

$$f_{29}(\bar{x},\bar{l}) = \dot{\bar{\beta}} \quad f_{30}(\bar{x},\bar{l}) = \dot{\bar{\varepsilon}} \quad f_{31}(\bar{x},\bar{l}) = \dot{\bar{h}}\Delta t + \ddot{\bar{\beta}}\Delta t \quad f_{32}(\bar{x},\bar{l}) = \dot{\bar{\varepsilon}}\bar{d}\Delta t$$

(3)

### 2.3.2 Intelligent navigation

Spatial information databases are now a standard component of many mobile navigation systems. This is directly due to their ability to provide detailed information about the location and inter-relationship of geographically defined features. Map matching techniques traditionally use this information in an attempt to improve navigation accuracy. This research proposes the integration of map matching techniques, (like other navigation instruments such as gyroscopes, odometers and GPS), within the Kalman filter, as a means of providing additional measurements that can be used to improve position and attitude determination. The map matching technique implemented in this research has been termed "Intelligent Navigation" (IN).

The IN algorithm developed in this research is modelled on the simple rules of navigation that humans use on a day-to-day basis, and in doing so incorporates both geometric and topological map matching techniques. This algorithm has several advantages; it consists of a simple, yet effective set of four rules (closest road, bearing matching, access only, distance in direction); it relies on the short term precision of the navigation sensors (in particular DR when GPS is unavailable); when implemented in the Kalman filter, IN has the unique advantage that it no longer assumes the navigator is on the road centreline (i.e. the road segments stored in the database), but instead is 'following' the road network. This is particularly important for high precision applications. No matter how accurate the database information, the navigator will not always travel directly on the network, but will travel to the left or right of the network to varying degrees (unless the navigator is fixed to the network as in the case of trains and trams).

The "closest road" rule of IN makes the assumption that the vehicle is travelling along a road (which is typically the case). This constraint can be included in the location solution, thus improving the accuracy of the computed position of the vehicle. This algorithm is most effective when the nearest road (according to the navigation instrument's computed position) is in fact the road being travelled. However, when approaching intersections or when two roads are close to each other, the nearest road may not be the road being travelled. In such cases, constraining the solution to fall on the nearest road actually downgrades the calculated position. To avoid such errors, the bearing matching rule is required. This rule requires that the nearest road to which the vehicle's position is corrected must have a bearing similar to the measured direction of travel. This corrects the problem previously described. The threshold of similarity between the vehicle's bearing and the bearing of the surrounding roads may be adjusted to suit the accuracy of the navigation instruments. However, the larger the threshold, the more likely it becomes that roads will be incorrectly matched as having the same bearing as that of the vehicle. The access only rule is designed to identify and prevent this error from occurring. Take, for example, a vehicle travelling along road A in the road layout diagram shown in Figure 4. Assuming the only route to road C is via road B, logic dictates that for the vehicle to be travelling along road C it must previously have travelled along road B. By logging previously travelled roads, the navigation system can prevent the vehicle from being located on a road that it could not possibly be on.

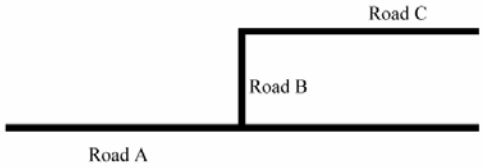


Figure 4 Road layout scenario

The distance in direction rule reduces the accumulation of distance error by calculating the distance travelled by the vehicle in the direction of the road rather than the direction measured by the navigation device. This is particularly important when navigation instruments of low accuracy are employed. For example, if a vehicle travels 1000 metres along a road of bearing 60 degrees while measuring the road to have a bearing of 65 degrees (i.e. 5 degrees in error), an error in distance of 4 metres will occur. Although this may seem insignificant, over several kilometres, or with lower accuracy navigation instruments, larger errors can accumulate. This error is avoided by calculating the distance travelled independently from the bearing of the vehicle and then applying this distance in the direction of the road being travelled.

### 2.3.3 Deriving the intelligent navigation observation equations

Incorporating IN into the Kalman filter requires the development of observation equations from the IN rules. This procedure also allows for additional parameters to be estimated by the filter, such as offset from the centreline. Furthermore, precisions can be associated with the information obtained from the map data to allow the Kalman filter to optimally estimate the position and attitude of the vehicle from all available measurements, rather than 'correcting' the vehicle's position to a point on the centreline.

The IN observation equations are derived from:

- the IN estimate of the vehicle's 'corrected' position (which lies on a road segment), and

- an estimate of the vehicle's heading (i.e. the heading of the road segment at the IN 'corrected' position).

An additional parameter is also added to the Kalman filter that estimates the shortest distance to the road segment that the vehicle is following (referred to as the Euclidean distance). By including this parameter, the IN rules no longer assume that the vehicle is directly on the road centreline, but instead follows a path parallel to the road centreline. The variance of this parameter dictates how closely the vehicle must follow the road centreline. The updated parameters for the state of the Kalman filter, including observations equations, are shown in Equations (7) and (8).

$$
\begin{aligned}
\bar{x}_i &= \left[\bar{E}\ \ \bar{N}\ \ \bar{U}\ \ \bar{h}\ \ \bar{p}\ \ \bar{r}\ \ \bar{v}\ \ \bar{\dot{h}}\ \ \bar{\dot{p}}\ \ \bar{\dot{r}}\ \ \bar{\dot{v}}\ \ \bar{\ddot{h}}\ \ \bar{\ddot{p}}\ \ \bar{\ddot{r}}\ \ \bar{\ddot{v}}\ \ \bar{\dddot{h}}\ \ \bar{\dddot{p}}\ \ \bar{\dddot{h}}\ \ \bar{\dddot{v}}\ \ \bar{\beta}\ \ \bar{\varepsilon}\ \ \bar{O}\right]^T \\
l_i &= \left[P_i\ \ e_i\right]^T \\
P_i &= \left[{}_pE\ \ {}_pN\ \ {}_pU\ \ {}_ph\ \ {}_pp\ \ {}_pr\ \ {}_pv\ \ {}_p\dot{h}\ \ {}_p\dot{p}\ \ {}_p\dot{r}\ \ {}_p\dot{v}\ \ {}_p\ddot{h}\ \ {}_p\ddot{p}\ \ {}_p\ddot{r}\ \ {}_p\ddot{v}\ \ {}_p\dddot{h}\ \ {}_p\dddot{p}\ \ {}_p\dddot{h}\ \ {}_p\dddot{v}\ \ {}_p\dot{\beta}\ \ {}_p\varepsilon\ \ {}_pO\right]^T \\
e_i &= \left[E^A\ \ N^A\ \ U^A\ \ E^B\ \ N^B\ \ U^B\ \ E^C\ \ N^C\ \ U^C\ \ \dot{h}\ \ d\ \ E^{IN}\ \ N^{IN}\ \ h^{IN}\right]^T
\end{aligned}
\tag{7}
$$

where:

| | |
|---|---|
| $O$ | Euclidean distance (m) from the road centreline (a prediction in $P_i$ and a parameter in the Kalman filter $\bar{x}_i$) |
| $E^{IN}$ | Easting coordinate (m) as measured from the road database |
| $N^{IN}$ | Northing coordinate (m) as measured from the road database |
| $h^{IN}$ | Heading (deg) as measured from the road database |

The resultant observation equations are as follows:

$$
\begin{aligned}
f_{32}\left(\bar{x},\bar{l}\right) &= \bar{O} \\
f_{33}\left(\bar{x},\bar{l}\right) &= \bar{E} + \bar{O}\sin\left(\bar{h}+90\right) \\
f_{34}\left(\bar{x},\bar{l}\right) &= \bar{N} + \bar{O}\cos\left(\bar{h}+90\right) \\
f_{35}\left(\bar{x},\bar{l}\right) &= \bar{h}
\end{aligned}
\tag{8}
$$

where:

| | |
|---|---|
| $f_{32}$ | Observation equation for the Euclidean distance from the road centreline as predicted by the Kalman filter |
| $f_{33}$ | Observation equation for the easting coordinate as measured from the road database |
| $f_{34}$ | Observation equation for the northing coordinate as measured from the road database |
| $f_{35}$ | Observation equation for the heading as measured from the road database |

### 2.3.4 Additional intelligent navigation parameters

There are three important additional parameters that can affect the operation of IN. These are:

- search radius,
- inner intersection exclusion radius, and
- angular similarity.

The search radius is the radial distance that the IN algorithm uses to search the surroundings for geospatial features. For example, given a search radius of 50 metres, at each estimated vehicle location, IN will search the surrounding area up to a radius of 50 metres for features such as roads and road intersections. The larger this distance, the larger the error that IN is able to correct for. If the nearest road is up to 50 metres away, IN (using a 50 metre search radius) is able to locate the road and update its estimated position to the road (if it meets the suitable criteria).

When approaching intersections, IN is switched off and the short term precision of the navigation instruments

(assuming DR navigation) is relied upon to avoid ambiguous situations. The proximity of intersections before IN is switched off is determined by the second parameter, inner intersection exclusion radius. The larger the radius, the more frequently intersections will be detected and IN corrections will therefore not occur.

The third parameter is the angular similarity. This refers to a tolerance within which the actual road bearing and calculated bearing (by the external navigation devices) are considered to be the same. As before, a larger value allows for larger errors to be corrected, but also increases the uncertainty in areas where roads intersect at oblique or acute angles.

In addition to these IN parameters, supplementary features have been added with the aim of further improving the accuracy of the navigation system. An additional parameter (the outer intersection exclusion radius) is used to constrain the operation of the IN algorithm, while a cornering algorithm allows for the use of IN on corners. IN could not previously implement the cornering algorithm, as prior to the inclusion of IN in the Kalman filter, an optimal estimate for the Euclidean distance to the road centreline was not available. This Euclidean distance is required to compute the trajectory of the vehicle through the corner.

The outer intersection exclusion radius parameter limits IN operation to the specified ranges of the inner intersection exclusion and outer intersection exclusion radii. For example, an inner intersection exclusion radius of 20m and outer intersection exclusion radius of 100m would limit IN operation to areas that are less than 100m but no closer than 20m to an intersection. This parameter is implemented in such a way that it also allows partial limitation of IN, for example, when the 'position exception' option is invoked, the position observations from the IN are included in the Kalman filter regardless of the outer intersection exclusion radius value. Similarly, using the 'heading exception' option allows heading observations to be included in the Kalman filter regardless of the outer intersection exclusion radius value.

All previous implementations of IN have not operated within the proximity of intersections (according to the inner intersection exclusion radius). As the vehicle travels through the intersection, IN does not provide any observations to the Kalman filter. The circular cornering algorithm overcomes this gap of observations by attempting to predict the vehicle's trajectory based on the available road centreline information. A circular curve is used as the prediction trajectory. Figure  illustrates this procedure. As the vehicle nears an intersection, the rate of turn of the vehicle is monitored. If the turn rate increases above a specified threshold, the intersection is examined to determine which road segment the vehicle is turning into. A circular curve is fitted to the vehicle's current position and predicted end of turn location. This curve is then used as the road centreline required by IN to provide observations. If the vehicle turns away from or continues to turn past the road the vehicle was predicted to follow, a new road prediction is made (again based on the vehicle's current position, heading, turn rate and data available in the road centreline database).

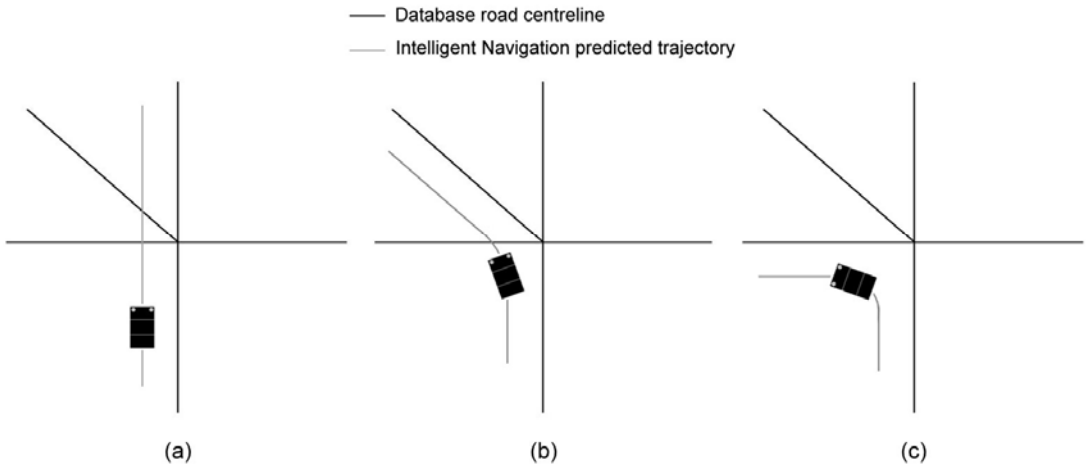


Figure 5 Circular cornering algorithm: (a) original trajectory prediction, (b) first updated trajectory prediction, and (c) second updated trajectory prediction

The only additional parameter required for the operation of the cornering algorithm is the turn rate threshold. This value indicates when the vehicle's turn rate is of a large enough magnitude to suggest that the vehicle is turning. All other information to predict the vehicle's trajectory is available either from the previous epoch of the Kalman filter or from the road centreline database. The method for calculating the IN position $\left(\mathrm{E}^{\mathrm{IN}}, \mathrm{N}^{\mathrm{IN}}\right)$ and heading $\left(\mathrm{h}^{\mathrm{IN}}\right)$ observables is shown in Figure and Equations 9. In order to compute the trajectory of the vehicle from one road to the next, an assumption is made that the Euclidean distance from the road centreline prior to the turn is the same once the turn has been completed.

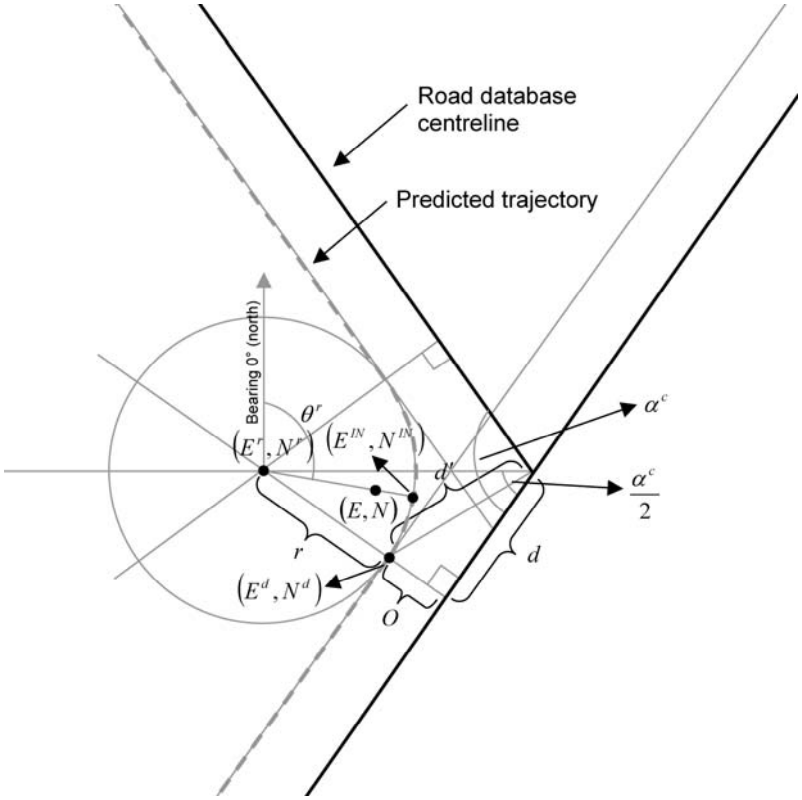


Figure6 Computing the turning radius and centre of rotation

$$
\begin{aligned}
\mathrm{d} &= \sqrt{\mathrm{d}'^2 - \mathrm{O}^2} \\
\mathrm{r} &= \mathrm{d}\tan\left(\frac{\alpha^{\mathrm{c}}}{2}\right) - \mathrm{O} \\
\theta^{\mathrm{r}} &= \arctan\left(\frac{\mathrm{E} - \mathrm{E}^{\mathrm{r}}}{\mathrm{N} - \mathrm{N}^{\mathrm{r}}}\right) \\
\mathrm{E}^{\mathrm{IN}} &= \mathrm{E}^{\mathrm{r}} + \mathrm{r}\sin\left(\theta^{\mathrm{r}}\right) \\
\mathrm{N}^{\mathrm{IN}} &= \mathrm{E}^{\mathrm{r}} + \mathrm{r}\cos\left(\theta^{\mathrm{r}}\right) \\
\mathrm{h}^{\mathrm{IN}} &= \left(\theta^{\mathrm{r}} - 90^{\circ}\right)
\end{aligned}
\tag{9}
$$

where

| | |
|---|---|
| O | Euclidean distance between Kalman filtered estimated position and IN estimated centreline position (provided by the Kalman filter) |
| $\left(\mathrm{E}^{\mathrm{d}}, \mathrm{N}^{\mathrm{d}}\right)$ | Point of deviation from the current road centreline (as determined by the turn rate threshold) |
| d′ | Distance from the road centreline intersection to the point of deviation (computed from the road centreline database) |

$(E, N)$ Vehicle position as computed by the navigation instruments

The additional parameters and algorithm detailed in this section significantly enhance the complexity of the resultant Kalman filter. The different modes that are now available within the IN module alone are summarised in **Error! Reference source not found.**1.

Table 1 Summary of Intelligent Navigation modes

| Mode | Description |
|---|---|
| Continuous | Provides position and heading estimations as inputs for the Kalman filter. Searches the database for road centrelines within the specified search radius, and with bearing matching the angular similarity constraint. Does not operate in areas where road intersections are within the intersection exclusion radius, but operates at all other times where road data is available. This mode includes the centreline offset that estimates the distance of the vehicle from the road centreline. Without this offset, an incorrect assumption would be made that the vehicle is travelling along the road centreline. |
| Outer intersection exclusion radius | Limits Intelligent Navigation operation to the specified ranges of the intersection inclusion and exclusion radii. For example, an inner intersection exclusion radius of 20m and outer intersection exclusion radius of 100m would limit Intelligent Navigation operation to areas that are less than 100m but no closer than 20m to an intersection. |
| Position exception | Allows input of Intelligent Navigation position estimation, overriding the outer intersection exclusion mode. |
| Heading exception | Allows input of Intelligent Navigation heading estimation, overriding the outer intersection exclusion mode. |
| Circular cornering algorithm | Estimates the turning path of the vehicle at road intersections and provides position and heading estimations throughout the curve. Operates only within the intersection exclusion radius. |

The processes for including IN information in the Kalman filter are shown in Figure 7. Using data from the GPS and DR instruments, the position and attitude of the vehicle are estimated. This information provides input for the IN algorithms. The results from IN are then combined with the GPS/DR measurements and filtered to provide an optimal solution using all available information. Note that there is only one Kalman filter, although it must be run twice. The first run provides the input for the IN algorithms. The second run computes the optimal state of the mobile platform using all available measurements (GPS, DR and IN).

The estimates of precisions used for the observations and the dynamic model are shown in Table 2.

Table 2 Precision estimates for the Kalman filter parameters

| **Dynamic model** | **Standard deviation** |
|---|---|
| $\dddot{h}$ | 0.001 deg/s$^5$ |
| $\ddot{p}$ | 0.01 deg/s$^3$ |
| $\dddot{r}$ | 0.01 deg/s$^3$ |
| $\dddot{v}$ | 0.001 m/s$^6$ |
| **Instrument measurement** | |
| Horizontal RTK GPS | 0.01m |
| Vertical RTK GPS | 0.02m |
| Gyro rate | 0.008deg/s |
| Odometer | 2% of distance measured |
| **Intelligent Navigation** | |
| $E^{IN}$ $N^{IN}$ | 0.1 metres |
| $h^{IN}$ | 1 degree |

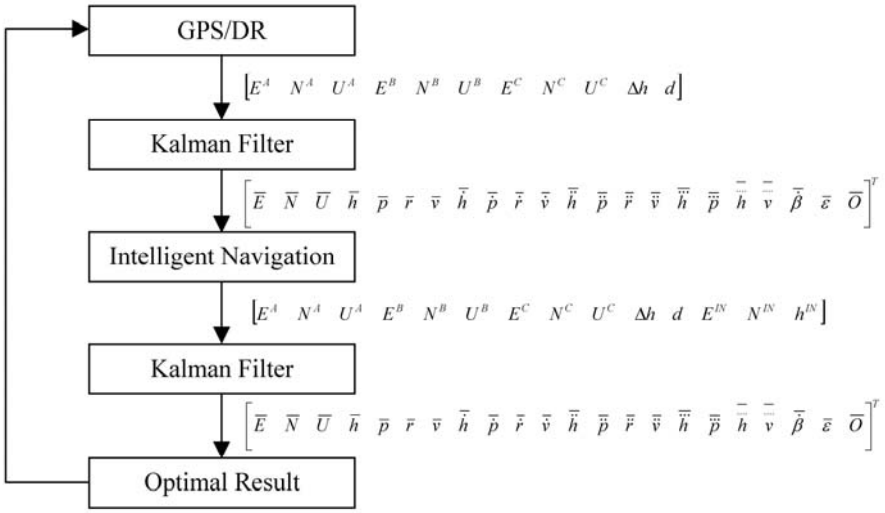


Figure 7 Kalman filter process with Intelligent Navigation

## 3 Testing and evaluation of Kalman filtering algorithms

To evaluate the integration algorithms developed in this research an AR prototype, ***i*ARM** (**I**ntelligent **A**ugmented **R**eality **M**apper) was constructed. The ***i*ARM** consists of the integrated positioning and attitude determination system described previously, combined with a digital video camera and a database containing three dimensional objects used for augmentation.

The ***i*ARM** was installed on a typical land mobile vehicle and a 1 kilometre road circuit located within the Melbourne General Cemetery was used as the test bed for this research. With an extensive network of roads, the cemetery offered many challenges to the integrated position and attitude determination system, as it contained GPS obstructions, as well as sharp corners and curving roads that continuously change the dynamics of the vehicle travelling the circuit. The location of road boundaries within the cemetery were predetermined and used to generate the objects used in the augmentation process.

The test vehicle was driven around the test circuit a number of times, with the AR prototype operating in real-time at 10 frames per second with VGA (640 × 480 pixels) resolution, and all navigation instruments operating. Figure 8 shows the AR prototype in operation with all sensors operating and the augmentation of the road boundaries.

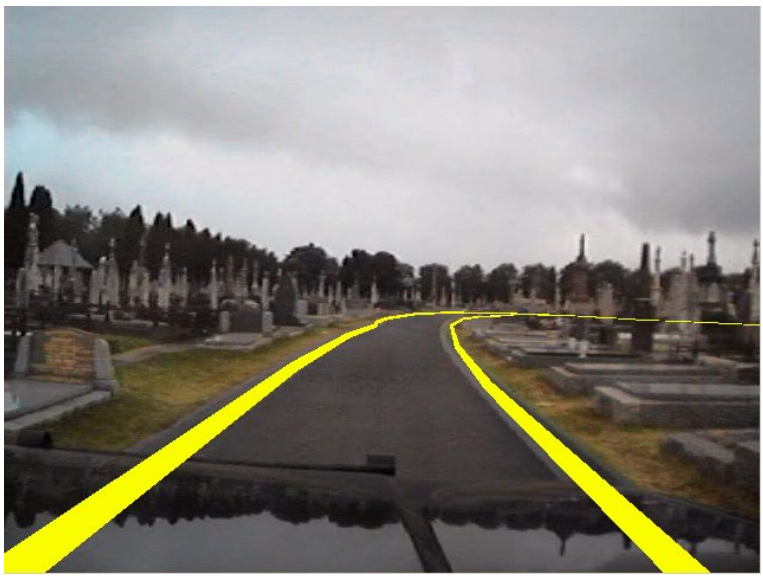

Figure 8 Augmented image from the prototype

From Figure 8 it is clearly visible that when all observations are available the integrated position and attitude determination system is successful in accurately aligning the augmented objects (the road boundaries) with the real world images of the driver as captured by the digital video camera. The results presented in Figure 8 are typical of the visual registration accuracy of augmented data and the real world images captured in this research.

In order to further explore and quantify the effects of errors in the position and attitude determination system, a single epoch of data from the vehicle travelling around the cemetery test circuit was selected. A 2 degree error was added to the heading as computed at that epoch. The augmented data was then rendered (using the heading with the error). The result is shown in Figure 9.

Figure 9 Misalignment of the augmented road boundaries caused by a 2 degree error in heading

As theoretically determined, the misalignment caused by an error in heading is more clearly obvious in the distance. However, the effect of foreshortening causes both the object being augmented as well as the augmented model to become smaller in the distance. Hence, misalignment of the most distant road boundary and augmented model cannot be visibly detected. In comparison, an error in position of 2 metres has the results shown in Figures 10 and 11.

Figure 10. Misalignment of the augmented road boundaries caused by a 2 metre position error that is perpendicular to the direction of travel

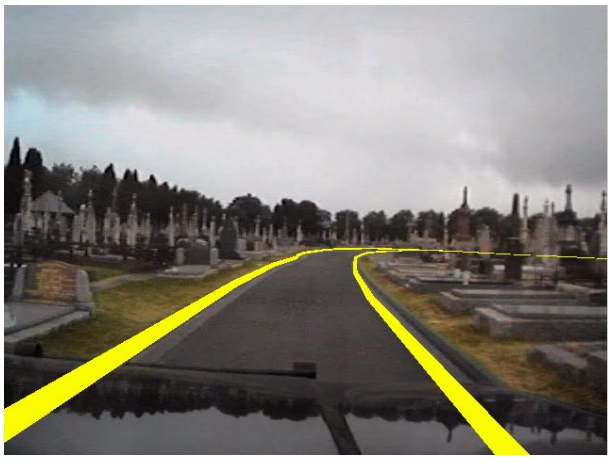

Figure 11. Misalignment of the augmented road boundaries caused by a 2 metre position error that occurs in the direction of travel

Despite the position errors shown in Figures 8 and 9 having exactly the same magnitude, the direction of the error has a profound effect. Where the error occurred in the direction of travel, very little visual effect could be

identified. On the other hand, when the direction of error was perpendicular to the direction of travel, the misalignment was clearly visible.

In order to evaluate the performance of the integrated position and attitude determination system during periods of GPS outages, a simulation test is conducted using the RTK GPS observations as a measure of the 'true' trajectory of the mobile platform. A portion of the data collected while travelling the test circuit was selected where RTK GPS observations were available. The GPS observations were then removed from the data, hence simulating a GPS outage. The simulated outage spanned 60 seconds. The Kalman filter was used to process the available DR measurements both with and without Intelligent Navigation. The alignment of augmented road boundaries exhibited by the AR prototype using only RTK GPS (i.e. the truth alignment), using only DR measurements (no IN), and using DR with IN are displayed in Figure 12.

Although Figure 12(b) shows a clear misalignment between the augmented and real road boundaries, the addition of the IN "observations" significantly reduces this misalignment as shown in Figure 12(c). In fact, as illustrated in Figure 13, the position error of the vehicle (calculated using the RTK GPS observations as truth) was reduced from 4.35 metres to 1.54 metres, a 65% reduction. It is important to note that despite a remaining position error of 1.54 metres after a 60 second outage, the alignment of the real and augmented boundaries appear visually correct as shown in Figure 12(c). The nature of the IN rules shift much of the remaining error in position into the direction of travel, hence minimising the visual misalignment caused by that error. This phenomenon is ultimately due to the linear nature of the road centrelines. This feature allows IN to readily detect and correct for errors perpendicular to the centreline, and without a change in heading (i.e. turning a corner), error in the direction of travel cannot be detected.

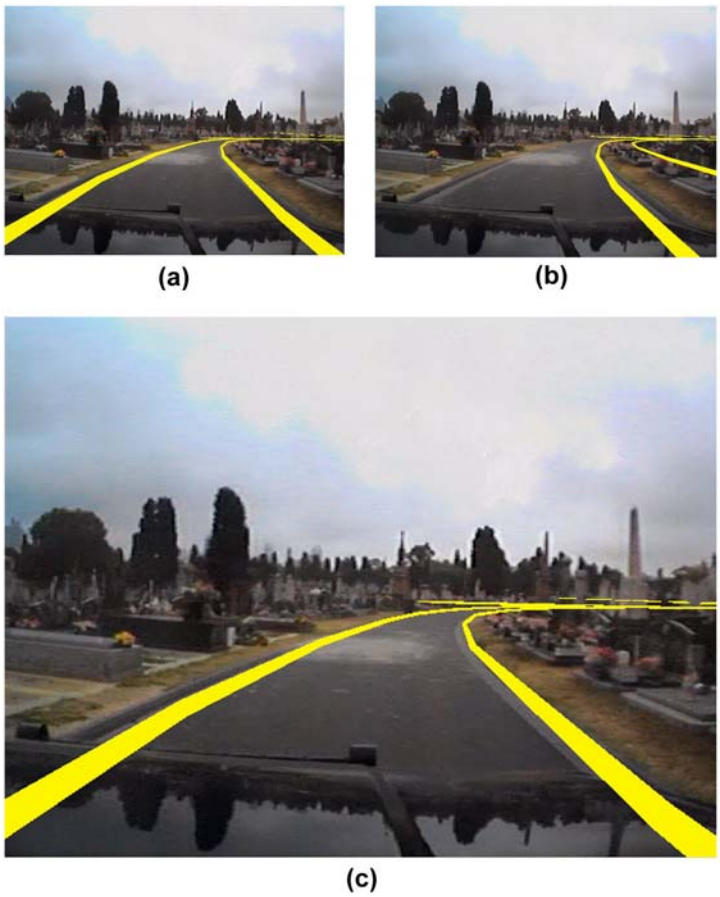


Figure 12 Augmentation of road boundaries using: (a) RTK GPS only, (b) integrated gyroscope and odometer after a 60 second GPS outage, and (c) integrated gyroscope, odometer and IN after a 60 second GPS outage

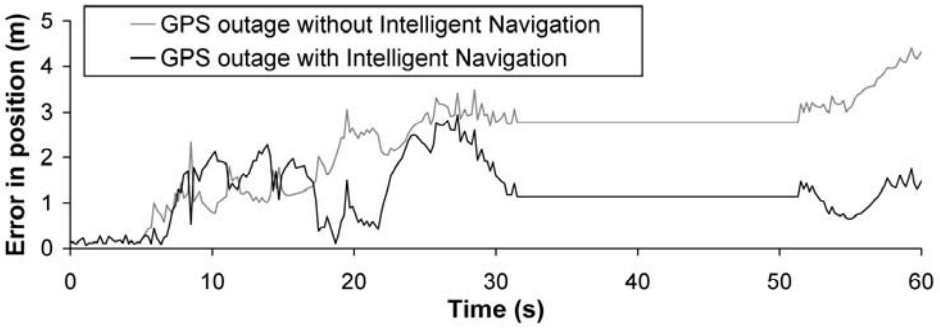


Figure 13 Position error over the 60 second GPS outage with and without IN

## 4 Conclusions

The aim of this research was to investigate the performance of an integrated position and attitude determination system to support AR applications in outdoor unprepared environments. To achieve this aim, multiple sensors and data sources were integrated within a Kalman filter. The position and attitude determination system was evaluated within a land mobile AR prototype developed within this research. Following are some of the conclusions drawn from this research.

- The Kalman filter developed was able to provide updates of position and attitude to enable accurate and continuous registration of the augmented objects with real world perspective views.
- The development of the unit variance test allowed for tuning of the Kalman filter to rapidly adapt to changes in the mobile platform dynamics. Hence the resulting filter provided improved results during times of low dynamics, but swift reaction times during high dynamics.
- The integration of the IN rules into the Kalman filter provided a significant improvement to position and attitude determination during GPS outages.
- The effect of errors in the position and attitude determination component on the alignment of augmented information with real world views was minimised when the error was contained primarily to the direction of travel. This occurrence is particularly relevant when considering the operation of IN. IN was found not only to reduce the magnitude of error, but to also constrain remaining error in the position solution to the direction of travel.

### References

Azuma R., Baillot Y., Reinhold B., Feiner S., Julier S., MacIntyre B. (2001) ***Recent Advances in Augmented Reality***, IEEE Computer Graphics and Applications, Vol. 21, No. 6, pp. 34-47.

Cross P.A. (1990) ***Advanced least squares applied to position-fixing***, Working Paper No. 6, Second Edition, North East London Polytechnic, Department of Land Surveying, London, United Kingdom.

Devernay F., Mourgues G., Coste-Maniere E. (2001) ***Towards endoscopic augmented reality for robotically assisted minimally invasive cardiac surgery***, Paper presented at the International Workshop on Medical Imaging and Augmented Reality, Shatin, Hong Kong, China, 10-12 July, 2001, 16-20.

Klinker G., Creighton O., Dutoit A., Kobylinski R., Vilsmeier C., Brugge B. (2001) ***Augmented maintenance of powerplants: A prototyping case study of a mobile AR system***, Paper presented at the IEEE and ACM International Symposium on Augmented Reality, New York, NY, USA, 124-133.

Logan S.A. (2000) ***Integration of GPS phase and other measurements for kinematic mapping***, Doctor of Philosophy Thesis, The University of Melbourne, Melbourne, Australia.